A Zero-Overhead ISAC Framework for Target Localization in Downlink MIMO-OFDM Networks

Ishita Sharma, Adarsh Patel
School of Computing and Electrical Engineering (SCEE), Indian Institute of Technology Mandi, Mandi, India
ud25010@students.iitmandi.ac.in, adarsh@iitmandi.ac.in

***Abstract*—This work presents an innovative integrated sensing and communications (ISAC) framework together with a novel Localization without Communication Overhead (LoCO) algorithm, which jointly realizes communication and sensing functionalities within state-of-the-art MIMO-OFDM communication networks. From a signal processing standpoint, the mathematical formulation of LoCO builds upon the Multiple Signal Classification (MUSIC) algorithm for angle-of-arrival (AoA) estimation. Furthermore, the proposed system incorporates a Hankelization procedure to exploit the inherent Vandermonde structure of the received signal snapshots, thereby enabling accurate round-trip delay estimation through rotational-invariance-based signal parameter estimation techniques. Numerical simulation results are provided to validate and quantify the superior localization performance of the proposed scheme. In particular, they show that advanced sensing capabilities can be achieved without any dedicated resource allocation, thereby preserving communication performance while simultaneously enabling high-resolution localization.**

***Index Terms*—Zero-overhead ISAC, target parameter estimation, MIMO-OFDM, localisation, MUSIC, Hankelisation, phased-array, signal processing.**

I. Introduction

Integrated Sensing and Communications (ISAC) refers to the synergistic combination of communication and sensing functionalities within a unified system architecture [1]. This convergence is primarily driven by the scarcity of available radio-frequency spectrum, the need for more efficient hardware utilization, and the associated benefits in terms of reduced cost and lower energy consumption [2]. ISAC is being incorporated into emerging sixth-generation (6G) standards because the International Mobile Telecommunications-2030 (IMT-2030) framework explicitly identifies joint sensing and communication capabilities as a key criterion for the functional completeness of 6G systems, in addition to the various performance and architectural advantages offered by such a unified approach [3], [4]. Representative application scenarios -including smart cities [5], vehicle-to-vehicle (V2V) communications [6], healthcare environments [7], precision agriculture [8], and drone detection [9] necessitate advanced platforms capable of providing high-reliability network connectivity while simultaneously supporting robust sensing functionalities.

The ISAC paradigm envisions next-generation communication networks endowed with real-time environmental sensing capabilities, wherein both base stations (BSs) and user equipments (UEs) actively participate in the sensing process [10]. Existing ISAC frameworks rely on various forms of signaling overhead to enable sensing functionality in wireless communication systems. Broadly, current research can be categorized according to the dominant source of overhead, encompassing works that employ precoding matrix design in conjunction with dedicated pilot symbols [11]–[13], pilot based sensing [14], [15], and as well as those that adopt resource partitioning strategies [16], [17] to support the coexistence of sensing and communication. However, these approaches have not yet realized fully integrated ISAC operation, as they are still predicated on the use of separate, rather than genuinely shared, communication and sensing resources.

Multiple studies in ISAC exploit precoding in conjunction with pilot-based techniques for joint sensing and communication. For example, [11] investigates a multiple-input multiple-output orthogonal frequency-division multiplexing (MIMO-OFDM) ISAC architecture that employs a common training structure to facilitate target sensing. In this framework, the authors design a transmit precoder that varies across OFDM frames to enable sensing while simultaneously transmitting pilot symbols. Building on this concept, [12] extends the methodology to terahertz (THz) systems, thereby enhancing sensing performance *via* tailored precoding and channel training sequences. In a complementary line of work, [13] combines pilot overhead with hybrid precoding to support radar sensing in parallel with communication beamforming. Other approaches rely primarily on pilot-based sensing; for instance, [14] introduces a dual-stage sensing strategy that employs isotropic downlink pilot signals for coarse sensing, followed by optimized directional pilot signals for fine-grained sensing. In a related overhead-oriented scheme, [15] proposes a pilot-transmission strategy designed to improve target detection probability under Quality of Service constraints.

The work presented in [16] introduces a multiuser MIMO ISAC framework that employs a differential subcarrier allocation strategy, in which a subset of subcarriers is reserved for sensing tasks while the entire set of subcarriers is utilized for communication. The study in [17] proposes an ISAC architecture that differentially allocates power and bandwidth resources between sensing and communication functionalities, thereby ensuring satisfactory sensing performance but at the expense of increased signaling and system overhead. Furthermore, the authors of [18] propose an ISAC strategy that uses the concept of shared and private subcarriers for localization, where all antennas transmit simultaneously on shared subcarriers, while one antenna per subcarrier restriction

on private subcarriers enables virtual array formation that improves the resolution of the angle estimate at the price of data throughput loss. The approaches motivate a critical examination of whether resource-partitioned architectures can be considered truly integrated sensing and communication systems, in the strict sense of jointly exploiting a common set of resources. A substantial body of research focuses on embedding sensing capabilities into communication networks, yet many such methods depend on additional overhead or dedicated resources, which undermines the core objective of using identical physical layer resources for both sensing and communication. Achieving high-quality sensing solely from standard communication signals remains a nontrivial challenge, and only a limited number of works directly address this problem. For example, the authors of [19] investigate the use of conventional communication waveforms for sensing in MIMO-OFDM systems, utilizing received echo signals, which could contain data-bearing symbols, to perform target localization.

This manuscript presents a novel algorithm, termed Localization without Communication Overhead (LoCO), specifically designed to localize a stationary point target situated between the BS and the UE. The algorithm operates exclusively on reflected echo components of downlink MIMO-OFDM data communication signals, thereby obviating the requirement for any additional sensing-specific waveform or signaling overhead. The proposed LoCO algorithm is structured as a two-stage processing framework. In the first stage, the data symbols are removed from the received echo signals, effectively isolating the channel-dependent components. In the second stage, the algorithm estimates the target localization parameters. For super-resolution estimation of the angle-of-arrival (AoA), LoCO employs the Multiple Signal Classification (MUSIC) [20]. Subsequently, a Hankelization procedure [21] is applied to exploit the inherent Vandermonde structure of the received signal model [22], which enables the use of the Estimation of Signal Parameters via Rotational Invariance Techniques [23] for accurate estimation of the round-trip time delay. The main contributions of this work are as follows:

- Introduction of a novel target Localization without Communication Overhead (LoCO) algorithm that addresses the fundamental problem of target localization in state-of-the-art MIMO-OFDM communication networks.
- Mathematical formulation of the LoCO algorithm for stationary target localization, wherein the estimated parameters comprise the radial range x inferred from the round-trip time delay τ, the azimuth angle θ, and the reflectivity coefficient α.
- Numerical simulation results are presented to validate and quantify the superior localization performance achieved by the proposed LoCO algorithm.

This manuscript adopts the following notational conventions: vectors and matrices are denoted in boldface lowercase and uppercase letters, respectively. A random vector $\mathbf{w} \sim \mathcal{CN}(\boldsymbol{\mu}, \boldsymbol{\Sigma})$ follows a complex Gaussian distribution

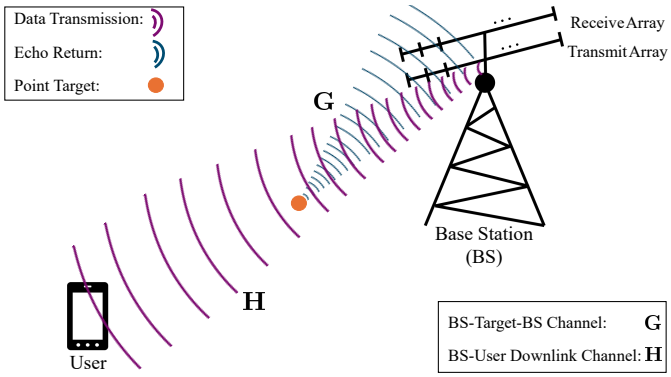

Fig. 1. An ISAC system model that deduces a stationary point target's localization parameters using the echo signal reflected back to the BS in a MIMO-OFDM framework.

characterized by a mean of $\boldsymbol{\mu}$ and a covariance matrix $\boldsymbol{\Sigma}$. The symbol $\mathbf{I}_N$ denotes the identity matrix of size $N \times N$, $j = \sqrt{-1}$ represents the imaginary unit, $|\cdot|$ denotes the magnitude, and $\|\cdot\|$ represents the Frobenius norm. The operators $(\cdot)^*$, $(\cdot)^T$, and $(\cdot)^H$ represent the complex conjugate, transpose, and Hermitian transpose, respectively. The symbols $\mathbb{R}$ and $\mathbb{C}$ are employed to denote real and complex fields, respectively. The vector $\mathbf{a} \in \mathbb{C}^{M\times 1}$ is defined as a complex vector, while $\mathbf{b} \in \mathbb{R}^{N\times 1}$ is a real vector.

The subsequent section introduces the ISAC framework in the context of MIMO-OFDM systems. The remainder of this manuscript is organized as follows. Section II provides a detailed description of the monostatic ISAC system model and the corresponding problem formulation. Section III presents the methodology employed to address the joint sensing-and-communication problem. In Section IV, the proposed approach is evaluated through numerical simulations. Finally, Section V summarizes the main contributions and outlines several promising directions for future research.

II. System Model

Consider a downlink MIMO-OFDM cellular communication system with a BS equipped with isolated uniform linear arrays (ULAs) comprising M transmit antennas and N receive antennas. The N receive antennas are employed to capture the echo signals reflected from a single stationary target or scatterer back towards the BS, as illustrated in Fig. 1. Both transmit and receive steering vectors assume a linear antenna array with uniform element spacing [24]. The transmit steering vector $\mathbf{a}_M(\phi) \in \mathbb{C}^{M\times 1}$, parameterized by the angle of departure (AoD) ϕ, and the receive steering vector $\mathbf{a}_N(\theta) \in \mathbb{C}^{N\times 1}$, parameterized by the angle of arrival (AoA) θ, are defined as

$$\mathbf{a}_M(\phi) = \frac{1}{\sqrt{M}}\left[1 \;\; e^{-j\frac{2\pi d}{\lambda_c}\sin\phi} \ldots e^{-j\frac{2\pi d}{\lambda_c}(M-1)\sin\phi}\right]^T \quad (1)$$

$$\mathbf{a}_N(\theta) = \frac{1}{\sqrt{N}}\left[1 \;\; e^{-j\frac{2\pi d}{\lambda_c}\sin\theta} \ldots e^{-j\frac{2\pi d}{\lambda_c}(N-1)\sin\theta}\right]^T, \quad (2)$$

respectively, where the spacing between the antennas in the ULA is denoted as $d = \lambda_c/2$ with carrier wavelength λ_c.

A. Downlink Communication Model

Consider each element of the transmit ULA at the BS as transmitting an independent binary phase shift keying (BPSK) symbol $\mathbf{s}_{p,k} \in \mathbb{C}^{M\times 1}$, where the element $[\mathbf{s}_{p,k}]_m \in \{+1, -1\}$ for $1 \leq m \leq M$. These symbols are transmitted over subcarrier index k, with $1 \leq k \leq K$, and within the OFDM frame indexed by p, with $1 \leq p \leq P$. The received signal vector $\check{\mathbf{r}}_{p,k} \in \mathbb{C}^{N_{UE}\times 1}$ at the UE, associated with the downlink communication channel $\mathbf{H}_{p,k} \in \mathbb{C}^{N_{UE}\times M}$ between the BS and the UE for the OFDM frame p and subcarrier k, where N_{UE} denotes the number of receive antennas at the UE, is formulated as

$$\check{\mathbf{r}}_{p,k} = \mathbf{H}_{p,k}\mathbf{s}_{p,k} + \check{\mathbf{w}}_{p,k}, \tag{3}$$

where the additive white Gaussian noise (AWGN) $\check{\mathbf{w}}_{p,k} \sim \mathcal{CN}\big(\mathbf{0},\, \sigma_w^2\mathbf{I}_{N_{UE}}\big)$. For downlink data detection in MIMO-OFDM networks, various techniques from the literature can be applied to the system model in (3). The target sensing methodology is outlined in the following subsection.

B. Echo Signal Sensing Model

Consider a point target/scatterer located between the BS and the UE. This point target reflects a portion of the downlink communication signal back toward the BS. The received echo signal $\tilde{\mathbf{r}}_{p,k} \in \mathbb{C}^{N\times 1}$ at the BS, arising from the reflection by a stationary target, can be expressed as

$$\tilde{\mathbf{r}}_{p,k} = \mathbf{G}_{p,k}\mathbf{s}_{p,k} + \tilde{\mathbf{w}}_{p,k}, \tag{4}$$

where $\tilde{\mathbf{w}}_{p,k} \sim \mathcal{CN}(\mathbf{0}, \sigma_w^2\mathbf{I}_N)$ is AWGN. The round-trip MIMO-OFDM channel $\mathbf{G}_{p,k} \in \mathbb{C}^{N\times M}$ in (4) for a stationary target follows the standard monostatic radar channel model [3] as

$$\mathbf{G}_{p,k} = \alpha e^{-j2\pi f_k \tau}\mathbf{a}_N(\theta)\mathbf{a}_M^H(\phi), \tag{5}$$

where f_k denotes the subcarrier frequency at index k, $\tau = 2x/c$ represents the round-trip propagation delay associated with a target located at radial range x, and $\alpha \in \mathbb{C}$ is the complex reflection coefficient. The transmit and receive steering vectors, $\mathbf{a}_M(\phi)$ and $\mathbf{a}_N(\phi)$, respectively, are defined according to the structures given in (1) and (2), with $\phi \neq \theta$. A nearby target may intercept part of the transmitted signal even if it is not exactly on the BS-UE line-of-site path. Thus, it is reasonable to assume $\phi \neq \theta$, since the target can lie at a different angle relative to the UE. The phase term induced by the carrier frequency is incorporated into α, such that $\alpha = |\alpha|e^{-j2\pi f_c \tau}$ [11]. The magnitude $|\alpha|$ of the reflection coefficient is modeled in accordance with the radar range equation [25], given by

$$|\alpha| = \sqrt{\frac{G_M G_N \lambda^2 \epsilon}{(4\pi)^3 x^4 \iota}}, \tag{6}$$

where G_M and G_N are transmit and receive antenna gains, λ is wavelength, ϵ is radar cross-section, and ι system losses. Substituting (5) in (4) the resulting received signal $\tilde{\mathbf{r}}_{p,k}$ is

$$\tilde{\mathbf{r}}_{p,k} = \alpha e^{-j2\pi f_k \tau}\mathbf{a}_N(\theta)\mathbf{a}_M^H(\phi)\mathbf{s}_{p,k} + \tilde{\mathbf{w}}_{p,k}. \tag{7}$$

The expression of $\tilde{\mathbf{r}}_{p,k}$ in (7) is subsequently employed in the target localization procedure described next.

III. Localization without Communication Overhead (LoCO) in downlink MIMO-OFDM

The BS has full knowledge of the transmitted BPSK-modulated data symbols $\mathbf{s}_{p,k}$ that are embedded in the received echo signals, since these echoes are generated by BS-originated waveforms and subsequently reflected by the target back to the BS. Given the BS beamforms the signal to UE, the AoD ϕ in (7) is presumed to be known *a priori*. The transmit and receive antenna arrays are assumed to be co-located at the BS and can attain ideal time-synchronization. The work in [19] assumes the transmit and receive arrays at the BS to be time-synchronized within the cyclic-prefix duration. The data-dependent factor that compensates for both the data symbols $\mathbf{s}_{p,k}$ and the transmit steering vector $\mathbf{a}_M(\phi)$, denoted by $\xi_{p,k}(\phi) = \mathbf{a}_M^H(\phi)\mathbf{s}_{p,k} \in \mathbb{C}$, is further expressed as

$$\xi_{p,k}(\phi) = \frac{1}{\sqrt{M}}\sum_{m=1}^{M} e^{j\frac{2\pi d}{\lambda_c}(m-1)\sin\phi}[\mathbf{s}_{p,k}]_m. \tag{8}$$

By substituting (8) into (7), received signal is reformulated as

$$\tilde{\mathbf{r}}_{p,k} = \alpha e^{-j2\pi f_k \tau}\xi_{p,k}(\phi)\mathbf{a}_N(\theta) + \tilde{\mathbf{w}}_{p,k}. \tag{9}$$

To eliminate the known data factor $\xi_{p,k}(\phi)$ in (9), the following operation is performed, yielding $\mathbf{r}_{p,k} \in \mathbb{C}^{N\times 1}$, illustrated as

$$\mathbf{r}_{p,k} = \frac{\xi_{p,k}^*(\phi)}{|\xi_{p,k}(\phi)|^2}\tilde{\mathbf{r}}_{p,k}. \tag{10}$$

By substituting (9) into (10), the known data symbols are eliminated, yielding

$$\mathbf{r}_{p,k} = \alpha e^{-j2\pi f_k \tau}\mathbf{a}_N(\theta) + \mathbf{w}_{p,k}, \tag{11}$$

where the modified noise is $\mathbf{w}_{p,k} = (\xi_{p,k}^*(\phi)/|\xi_{p,k}(\phi)|^2)\tilde{\mathbf{w}}_{p,k}$ and follows a complex PDF, i.e., $\mathbf{w}_{p,k} \sim \mathcal{CN}\left(\mathbf{0}, \frac{\sigma_w^2}{|\xi_{p,k}(\phi)|^2}\mathbf{I}_N\right)$.

A. Target Parameter Estimation

Given the processed echo signal in (11), the objective is to estimate the localization parameters of the stationary point target, namely the AoA (ϕ), range (x), and reflectivity coefficient (α).

1) AoA Estimation: To enhance the signal-to-noise ratio (SNR), an averaging operation over P consecutive OFDM frames is performed as

$$\mathbf{r}_k = \frac{1}{P}\sum_{p=1}^{P}\mathbf{r}_{p,k} = \alpha e^{-j2\pi f_k \tau}\mathbf{a}_N(\theta) + \mathbf{w}_k, \tag{12}$$

where $\mathbf{w}_k = \frac{1}{P}\sum_{p=1}^{P}\mathbf{w}_{p,k}$ with $\mathbf{w}_k \sim \mathcal{CN}\left(\mathbf{0}, \eta_k^2\mathbf{I}_N\right)$ and $\eta_k^2 = \frac{\sigma_w^2}{P^2}\sum_{p=1}^{P}|\xi_{p,k}(\phi)|^{-2}$. Using (12) the spatial covariance matrix $\mathbf{C}_r \in \mathbb{C}^{N\times N}$ across K subcarriers can be evaluated as $\mathbf{C}_r = \frac{1}{K}\sum_{k=1}^{K}\mathbf{r}_k\mathbf{r}_k^H$ which has the following structure:

$$\mathbf{C}_r = |\alpha|^2\mathbf{a}_N(\theta)\mathbf{a}_N^H(\theta) + \sigma_n^2\mathbf{I}_N. \tag{13}$$

The effective noise variance $\sigma_n^2 = \frac{1}{K^2}\sum_{k=1}^{K}\eta_k^2$ denoting the average across all OFDM frames and subcarriers. The Multiple Signal Classification (MUSIC) [20] algorithm is employed to obtain super-resolution estimates of the direction-of-arrival (DoA). This method exploits the orthogonality between the signal and noise subspaces to perform angular estimation. Specifically, after computing the eigenvalue decomposition of the covariance matrix $\mathbf{C}_r$ in (13) as $\mathbf{C}_r = \sum_{n=1}^{N}\rho_n\mathbf{z}_n\mathbf{z}_n^H$, where $\rho_1 \geq \rho_2 \geq \cdots \geq \rho_N$ denote the eigenvalues in non-increasing order and $\{\mathbf{z}_n\}_{n=1}^{N}$ are the corresponding eigenvectors, the signal and noise subspaces can be identified. For a single point target, the signal subspace is one-dimensional and is spanned by $\mathbf{z}_1$, which is associated with the largest eigenvalue ρ_1, while the noise subspace is spanned by the remaining eigenvectors $\{\mathbf{z}_2, \mathbf{z}_3, \ldots, \mathbf{z}_N\}$. The noise subspace matrix $\mathbf{Z}_{\mathrm{n}} \in \mathbb{C}^{N\times(N-1)}$ is thus constructed as

$$\mathbf{Z}_{\mathrm{n}} = \begin{bmatrix}\mathbf{z}_2 & \mathbf{z}_3 & \cdots & \mathbf{z}_N\end{bmatrix}. \tag{14}$$

To compute the MUSIC pseudospectrum $\boldsymbol{\kappa}(\theta')$, proceed according to step (3) of the proposed algorithm presented in Algorithm 1. Specifically, employ the analytical expression for the pseudospectrum $\boldsymbol{\kappa}(\theta')$ to evaluate its values over the desired angular grid. AoA is now estimated using the optimization problem defined as

$$\hat{\theta} = \arg\max_{\theta'\in\Theta}\boldsymbol{\kappa}(\theta'), \tag{15}$$

where Θ in (15) denotes the discretized angular domain comprising the candidate azimuth angles.

2) Time Delay Estimation: Subsequently, based on the estimated AoA $\hat{\theta}$, conjugate beamforming is performed to obtain $y_{p,k} = \mathbf{a}_N^H(\hat{\theta})\mathbf{r}_{p,k}$, thereby compensating for the spatial steering effect and enabling the subsequent estimation of the remaining target parameters. The beamformed signal is

$$y_{p,k} = \alpha e^{-j2\pi f_k\tau} + w_{p,k}, \tag{16}$$

where $w_{p,k} = \mathbf{a}_N^H(\hat{\theta})\mathbf{w}_{p,k} \sim \mathcal{CN}\left(0, \frac{N\sigma_w^2}{|\xi_{p,k}(\phi)|^2}\right)$ is noise. The signal (16) can be averaged over P OFDM frames to give

$$y_k = \frac{1}{P}\sum_{p=1}^{P} y_{p,k} = \alpha e^{-j2\pi f_k\tau} + w_k, \tag{17}$$

where $w_k \sim \mathcal{CN}\left(0, \frac{N\sigma_w^2}{P^2}\sum_{p=1}^{P}\frac{1}{|\xi_{p,k}(\phi)|^2}\right)$. The signal y_k now contains only the reflection coefficient α and time delay τ, from which the range can be estimated. The signal in (17) exhibits a Vandermonde structure [22] in the frequency domain because the subcarrier frequencies satisfy $f_k = k\Delta f$, where Δf denotes the subcarrier spacing and k is the subcarrier index. To preserve this Vandermonde structure and enable subsequent parameter estimation via rotational invariance [23], a Hankel matrix [21] $\mathbf{E} \in \mathbb{C}^{L\times T}$ is constructed with window length $L = \lfloor K/2 \rfloor$ and $T = K - L + 1$ columns, where $\lfloor\cdot\rfloor$ denotes the floor function. The entries of the Hankel matrix $\mathbf{E}$ are $[\mathbf{E}]_{l,t} = y_{l+t-1}$. Let $\mathbf{u}_1$ denote the dominant (first) left singular vector of $\mathbf{E}$. The selection matrices are then given as

$$\mathbf{Q}_1 = [\mathbf{I}_{L-1}, \mathbf{0}] \in \mathbb{R}^{(L-1)\times L}, \quad \mathbf{Q}_2 = [\mathbf{0}, \mathbf{I}_{L-1}] \in \mathbb{R}^{(L-1)\times L},$$

where $\mathbf{0}$ denotes a zero matrix of appropriate dimension. The round-trip time-delay estimate $\hat{\tau}$ is subsequently inferred from the complex rotational factor $\psi \in \mathbb{C}$, which is obtained through the associated rotational invariance operation

$$\psi = \frac{(\mathbf{Q}_1\mathbf{u}_1)^H\mathbf{Q}_2\mathbf{u}_1}{\|\mathbf{Q}_1\mathbf{u}_1\|^2}. \tag{18}$$

Therefore, using the rotational operator defined in (18), the time delay $\hat{\tau}$ can be estimated as

$$\hat{\tau} = -\frac{\angle(\psi)}{2\pi\Delta f}, \tag{19}$$

where $\angle(\cdot)$ denotes the phase angle operator. Furthermore, by substituting the estimated time delay $\hat{\tau}$ obtained from (19), the radial distance to the target can be computed as $\hat{x} = c\hat{\tau}/2$, where c represents the speed of light.

3) Reflectivity Coefficient Estimation: The phase rotation induced by the propagation delay in (16) can be compensated by employing the time-delay estimate $\hat{\tau}$ from (19), yielding the corrected observation $\tilde{y}_{p,k} = y_{p,k}\, e^{j2\pi f_k\hat{\tau}}$. By expanding this expression, one obtains

$$\tilde{y}_{p,k} \approx \alpha + w_{p,k}e^{j2\pi f_k\hat{\tau}}, \tag{20}$$

which takes into account $\hat{\tau} \approx \tau$. The reflection coefficient $\hat{\alpha}$ can then be estimated by averaging over all OFDM frames and subcarrier frequencies as

$$\hat{\alpha} = \frac{1}{PK}\sum_{p=1}^{P}\sum_{k=1}^{K}\tilde{y}_{p,k}. \tag{21}$$

The target localization without communication overhead (LoCO) algorithm for ISAC in downlink MIMO-OFDM is delineated in Algorithm 1. The following section presents an analysis of the simulation results.

Algorithm 1 Target LoCO for ISAC in MIMO-OFDM

Input: Received echo signal $\tilde{\mathbf{r}}_{p,k}$, data symbol vector $\mathbf{s}_{p,k}$, AoD ϕ, angular grid Θ, subcarrier spacing Δf, and window length $L = \lfloor K/2 \rfloor$.

Output: Target localization parameters $\hat{\theta}$, $\hat{\tau}$, $\hat{x}$, and $\hat{\alpha}$.

Echo Signal Conditioning

Form $\xi_{p,k}(\phi) \leftarrow \frac{1}{\sqrt{M}}\sum_{m=1}^{M} e^{j\frac{2\pi d}{\lambda_c}(m-1)\sin\phi}[\mathbf{s}_{p,k}]_m$

Data removal $\mathbf{r}_{p,k} \leftarrow \frac{\xi_{p,k}^*(\phi)}{|\xi_{p,k}(\phi)|^2}\tilde{\mathbf{r}}_{p,k}$. *// use* (9) *for* $\tilde{\mathbf{r}}_{p,k}$

Target Parameter Estimation

Form $\boldsymbol{\kappa}(\theta') = \frac{1}{\mathbf{a}_N^H(\theta')\mathbf{Z}_n\mathbf{Z}_n^H\mathbf{a}_N(\theta')}$ *// get* $\mathbf{Z}_n$ *via* (14)

Estimate $\hat{\theta} \leftarrow \arg\max_{\theta'\in\Theta}\boldsymbol{\kappa}(\theta')$

Conjugate beamform $y_{p,k} \leftarrow \mathbf{a}_N^H(\hat{\theta})\mathbf{r}_{p,k}$

Estimate $\hat{\tau} \leftarrow -\frac{\angle(\psi)}{2\pi\Delta f}$ *// get* (ψ) *via* (18)

Estimate $\hat{x} \leftarrow c\hat{\tau}/2$

Estimate $\hat{\alpha} \leftarrow \frac{1}{PK}\sum_{p=1}^{P}\sum_{k=1}^{K}\tilde{y}_{p,k}$. *// get* $\tilde{y}_{p,k}$ *via* (20)

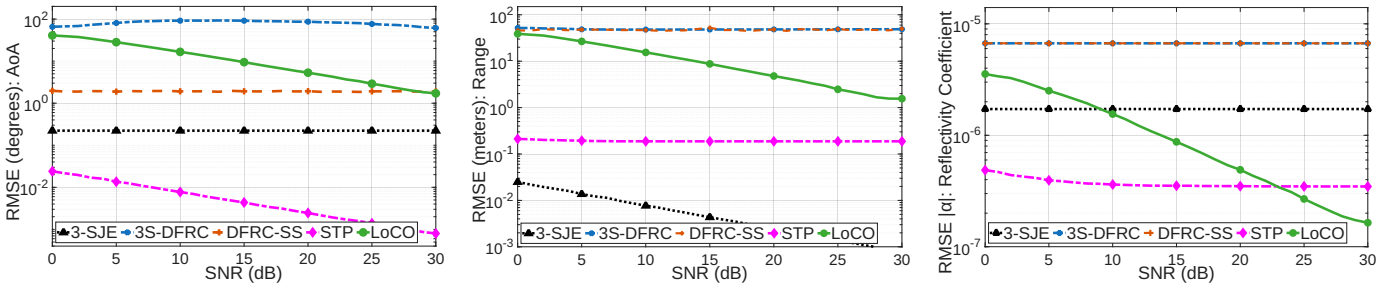

(a) (b) (c)

Fig. 2. Performance comparison with respect to the NMSE vs. SNR of the proposed LoCO algorithm and the existing ISAC methods—such as 3-SJE [19], 3S-DFRC [13], DFRC-SS [18], and STP [11] based ISAC schemes for the estimates of (a) angle, (b) range, (c) reflection coefficient.

IV. Simulation Results

A. State-of-the-art techniques

To validate the performance of the proposed algorithm LoCO, for target localization, a comparative analysis is performed against two categories of ISAC techniques. The first category employs a zero-overhead approach but uses a different signal processing methodology, specifically the 3-Step Joint Estimation (3-SJE) [19]. The 3-SJE method uses Discrete Fourier Transform (DFT)-based spectral analysis to estimate the target angle. After obtaining the angle estimate, angle-dependent signal terms are removed, and range is then extracted via additional 2D-DFT spectral analysis. The second category includes overhead-based ISAC techniques that utilize additional resources namely, Dual Functional Radar Communication with Shared-Subcarriers (DFRC-SS) [18], Shared Training Pattern (STP) strategy [11] and 3-Stage Dual Functional Radar Communication (3S-DFRC) estimation [13]. The DFRC-SS technique employs a two-stage angle-of-arrival estimation procedure. In the first stage, a coarse estimate of the angle is obtained using a discrete Fourier transform (DFT)-based method. In the subsequent refinement stage, this preliminary estimate is improved through sparse signal recovery techniques. The refinement step operates on a virtual array that is synthesized from the signals corresponding to the private subcarriers. However, the division of subcarriers into shared and private sets introduces additional overhead. Specifically, a subset of subcarriers must be designated as private, such that, at any given time, each of these subcarriers is constrained to be transmitted from only a single antenna, whereas the shared subcarriers are transmitted simultaneously from all antennas. In the STP strategy, a precoded training structure is used, with the training precoder matrix designed to enable tensor decomposition for target localization. However, this STP strategy requires dedicated training resources, contradicting the core idea of zero-overhead sensing-communication integration. The 3S-DFRC estimation operates in three sequential stages within each Pulse Repetition Interval. It employs Linear Frequency Modulated pilot signals instead of data symbols for target localization, thus consuming a significant portion of resources to integrate sensing with communication.

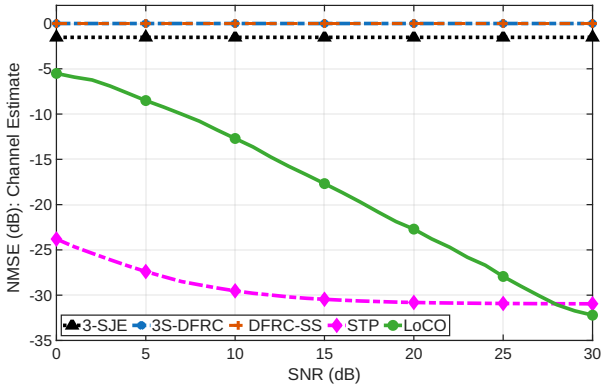

Fig. 3. NMSE vs. SNR channel estimate performance comparison of the proposed LoCO algorithm with the 3-SJE [19], 3S-DFRC [13], DFRC-SS [18], and STP [11] schemes.

B. Simulation Setup and Results

Consider an ISAC architecture in downlink MIMO-OFDM [11] with the BS equipped with ULAs consisting of 64 transmit and receive antennas, respectively. This framework operates at a carrier frequency f_c = 28GHz with a bandwidth of 100MHz. The configuration uses 128 OFDM subcarriers that have a spacing $\Delta f = 781.25$ kHz. The duration of the OFDM symbol is $T_S = 1.28\mu$s and the cyclic prefix time is given as $T_{CP} = 0.64\mu$s. The BS transmits $P = 32$ OFDM frames and utilizes $K = 16$ active subcarriers. The magnitude of the reflection coefficient given in (6) is parameterized by $G_M = G_N = 64$, $\epsilon = 1$ m^2, and $\iota = 1$.

Fig. 2(a) illustrates the Root Mean Square Error (RMSE) performance of Algorithm 1 under the considered techniques. LoCO outperforms 3S-DFRC owing to its super-resolution angle-of-arrival (AoA) estimation procedure based on the MUSIC algorithm, which then converges with DFRC-SS, which achieves superior performance because of its two-step angle estimation process. In contrast, the 3S-DFRC scheme, while also relying primarily on MUSIC for angle estimation, suffers from reduced performance because the number of available observations is limited by the reliance on dedicated pilots. The 3-SJE technique achieves a better performance because of its DFT-based estimation technique. Furthermore, the carefully

designed training precoder matrix in STP with random phases enables effective tensor decomposition, thereby improving estimation accuracy at the cost of increased resource overhead.

Fig. 2(b) presents the Root Mean Square Error (RMSE) in range estimation. LoCO exhibits superior performance compared to 3S-DFRC and DFRC-SS, primarily due to its rotationally invariant estimation strategy. STP further leverages its specifically designed training structure in conjunction with a rotationally invariant estimation method to achieve a lower RMSE. 3-SJE exploits a two-dimensional discrete Fourier transform (DFT) along the fast-time (subcarrier) and slow-time (OFDM symbol) dimensions to jointly estimate range and velocity (with velocity being zero for a stationary target) to attain the best overall estimation accuracy.

Fig. 2(c) presents RMSE for reflectivity-coefficient estimates. LoCO gives better estimation performance than 3S-DFRC and DFRC-SS throughout all the SNRs while giving the best estimation performance among all the techniques at high SNRs. STP gives a stable performance because of its consistent performance in estimating the previous parameters.

The overall channel estimation performance is illustrated in Fig. 3 *via* Normalized Mean Square Error (NMSE) *vs.* SNR plot. LoCO performs better in comparison to 3-SJE, 3S-DFRC and DFRC-SS while later converging with STP at high SNR because it employs stable estimation methods for each of the parameter being estimated. STP performs better till roughly 27dB SNR but depends on precoded training structure, incompatible of estimating parameters from data embedded echo signals. The results conclude that LoCO achieves a substantial localization performance.

V. Conclusion and Future Work

This work proposed a zero-overhead-based ISAC algorithm, referred to as LoCO, in MIMO-OFDM systems. In contrast to conventional schemes that require additional dedicated resources and impose constraints on system architecture, the LoCO algorithm exploits the naturally occurring echo reflections of the communication signals for target localization. While this work focused on a single-user scenario with a stationary target, various avenues for future work exist, including scenarios with multiple users, simultaneous detection of several targets, and parameter estimation of a moving target. The proposed LoCO algorithm achieves target localization by exploiting only the received echo signal without necessitating the use of external overhead for target localization.

References

[1] T. Liu, K. Guan, D. He, P. T. Mathiopoulos, K. Yu, Z. Zhong, and M. Guizani, "6G Integrated Sensing and Communications Channel Modeling: Challenges and Opportunities," *IEEE Veh. Technol. Mag.*, vol. 19, no. 2, pp. 31–40, 2024.

[2] J. A. Zhang, F. Liu, C. Masouros, R. W. Heath, Z. Feng, L. Zheng, and A. Petropulu, "An Overview of Signal Processing Techniques for Joint Communication and Radar Sensing," *IEEE J. Sel. Topics Signal Process.*, vol. 15, no. 6, pp. 1295–1315, 2021.

[3] F. Liu, Y. Cui, C. Masouros, J. Xu, T. X. Han, Y. C. Eldar, and S. Buzzi, "Integrated Sensing and Communications: Toward Dual-Functional Wireless Networks for 6G and Beyond," *Proc. IEEE J. Sel. Areas Commun.*, vol. 40, no. 6, pp. 1728–1767, 2022.

[4] A. Kaushik, R. Singh, S. Dayarathna, R. Senanayake, M. D. Renzo, M. Dajer, H. Ji, Y. Kim, V. Sciancalepore, A. Zappone, and W. Shin, "Toward Integrated Sensing and Communications for 6G: Key Enabling Technologies, Standardization, and Challenges," *IEEE Commun. Stand. Mag.*, vol. 8, no. 2, pp. 52–59, 2024.

[5] D. Milovanovic, G. Gardasevic, V. Terzija, and Q. Li, "Study on 6G Use Cases and Service Requirements for Future Cities," in *Proc. 8th Int. Balkan Conf. Commun. Netw. (BalkanCom)*, 2025, pp. 1–5.

[6] A. U. Khan, S. J. Myint, S. N. H. Shah, C. Schneider, and J. Robert, "Exploring the Impact of Bistatic Target Reflectivity in ISAC-Enabled V2V Setup Across Diverse Geometrical Road Layouts," *IEEE Open J. Veh. Technol.*, vol. 6, pp. 948–968, 2025.

[7] Y. Zhang, C. Masouros, and T. Xu, "Zero-Power Integrated Sensing and Communication in Smart Healthcare Environments," *IEEE Trans. Cogn. Commun. Netw.*, vol. 11, no. 5, pp. 3079–3093, 2025.

[8] X. Zhang, R. Zhang, Y. Cui, M. Gao, W. Yuan, and X. Jing, "AGI-Enabled Networked Sensing Data Aggregation for Heterogeneous UAV-UGV Coalition in Low-Altitude ISAC Systems," *IEEE Trans. Cogn. Commun. Netw.*, pp. 1–1, 2025.

[9] S. Jana, A. K. Mishra, and M. Z. A. Khan, "Opportunistic Drone Detection Using CommSense," *IEEE Trans. Instrum. Meas.*, vol. 74, pp. 1–15, 2025.

[10] N. Kim, J. Han, J. Choi, A. Alkhateeb, C.-B. Chae, and J. Park, "Integrated Sensing and Communications in Downlink FDD MIMO without CSI Feedback," *IEEE Trans. Wireless Commun.*, pp. 1–1, 2025.

[11] R. Zhang, L. Cheng, S. Wang, Y. Lou, Y. Gao, W. Wu, and D. W. K. Ng, "Integrated Sensing and Communication With Massive MIMO: A Unified Tensor Approach for Channel and Target Parameter Estimation," *IEEE Trans. Wireless Commun.*, vol. 23, no. 8, pp. 8571–8587, 2024.

[12] R. Zhang, X. Wu, Y. Lou, F.-G. Yan, Z. Zhou, W. Wu, and C. Yuen, "Channel-Training-Aided Target Sensing for Terahertz Integrated Sensing and Massive MIMO Communications," *IEEE Internet Things J.*, vol. 12, no. 4, pp. 3755–3770, 2025.

[13] F. Liu, C. Masouros, A. P. Petropulu, H. Griffiths, and L. Hanzo, "Joint Radar and Communication Design: Applications, State-of-the-Art, and the Road Ahead," *IEEE Trans. Commun.*, vol. 68, no. 6, pp. 3834–3862, 2020.

[14] Z. Huang, K. Wang, A. Liu, Y. Cai, R. Du, and T. X. Han, "Joint Pilot Optimization, Target Detection and Channel Estimation for Integrated Sensing and Communication Systems," *IEEE Trans. Wireless Commun.*, vol. 21, no. 12, pp. 10 351–10 365, 2022.

[15] M. Hua, Q. Wu, W. Chen, A. Jamalipour, C. Wu, and O. A. Dobre, "Integrated Sensing and Communication: Joint Pilot and Transmission Design," *IEEE Trans. Wireless Commun.*, vol. 23, no. 11, pp. 16 017–16 032, 2024.

[16] N. T. Nguyen, N. Shlezinger, Y. C. Eldar, and M. Juntti, "Multiuser MIMO Wideband Joint Communications and Sensing System With Subcarrier Allocation," *IEEE Trans. Signal Process.*, vol. 71, pp. 2997–3013, 2023.

[17] F. Dong, F. Liu, Y. Cui, W. Wang, K. Han, and Z. Wang, "Sensing as a Service in 6G Perceptive Networks: A Unified Framework for ISAC Resource Allocation," *IEEE Trans. Wireless Commun.*, vol. 22, no. 5, pp. 3522–3536, 2023.

[18] Z. Xu and A. Petropulu, "A Bandwidth Efficient Dual-Function Radar Communication System Based on a MIMO Radar Using OFDM Waveforms," *IEEE Trans. Signal Process.*, vol. 71, pp. 401–416, 2023.

[19] Z. Xiao, R. Liu, M. Li, Q. Liu, and A. L. Swindlehurst, "A Novel Joint Angle-Range-Velocity Estimation Method for MIMO-OFDM ISAC Systems," *IEEE Trans. Signal Process.*, vol. 72, pp. 3805–3818, 2024.

[20] R. Schmidt, "Multiple Emitter Location and Signal Parameter Estimation," *IEEE Trans. Antennas Propag.*, vol. 34, no. 3, pp. 276–280, 1986.

[21] N. Golyandina, V. Nekrutkin, and A. A. Zhigljavsky, *Analysis of Time Series Structure: SSA and Related Techniques*. Boca Raton, FL, USA: Chapman and Hall/CRC, 2001.

[22] G. H. Golub and C. F. Van Loan, *Matrix Computations*, 3rd ed. Baltimore, MD and London: The Johns Hopkins University Press, 1996.

[23] R. Roy and T. Kailath, "ESPRIT-Estimation of Signal Parameters Via Rotational Invariance Techniques," *IEEE Trans. Acoust., Speech, Signal Process.*, vol. 37, no. 7, pp. 984–995, 1989.

[24] H. Krim and M. Viberg, "Two decades of array signal processing research: the parametric approach," *IEEE Signal Process. Mag.*, vol. 13, no. 4, pp. 67–94, 1996.

[25] M. A. Richards, J. A. Scheer, and W. A. Holm, *Principles of Modern Radar: Basic Principles*. London, U.K.: IET, 2010.